

Double contact analysis of multilayered elastic structures involving functionally graded materials

J. YAN, C. MI

*Jiangsu Key Laboratory of Engineering Mechanics
School of Civil Engineering
Southeast University
Nanjing, Jiangsu 210096, China
e-mail: mi@seu.edu.cn*

THIS PAPER ANALYZES THE FRICTIONLESS DOUBLE CONTACT PROBLEM of a two-layer laminate pressed against a homogeneous half-plane substrate by a rigid punch. The laminate is composed of a homogeneous elastic strip and a functionally graded layer, perfectly bonded along their interface. The mechanical properties of the graded layer are modeled by an exponentially varying shear modulus and constant Poisson's ratio. Both the governing equations and the boundary conditions of the double contact problem are converted into a pair of singular integral equations by Fourier integral transforms, which are numerically integrated by Chebyshev–Gauss quadrature. The contact pressure and the contact size at both the advancing and the receding contact interface are eventually obtained by an iterative algorithm, developed from the method of steepest descent. Extensive parametric studies suggest that it is possible to control contact stress and contact size by introducing functionally graded materials into multilayered elastic structures.

Key words: functionally graded material, receding contact, double contact, rigid stamp, singular integral equations.

Copyright © 2017 by IPPT PAN

1. Introduction

THE MATERIAL PROPERTIES AND/OR FUNCTIONS of functionally graded materials (FGMs) are typically allowed to vary along one or more dimensions [1]. FGMs have been invented in the 1980s and have found their applications in materials science, mechanical engineering, and aerospace engineering, among other scientific and engineering fields. They often act as a transitional medium bridging the load-bearing elements and the exterior coating of an engineering structure. For example, in self-lubricating sliding bearings voids are used to store lubricants. More voids help to better lubricate the sliding surface but typically result in lower load-bearing capacity. To solve this contradiction, the void concentration is now designed to continuously change along the radial axis of a bearing. FGMs can also be directly employed as coatings. In both scenarios, FGMs help to prevent primary components from excessive degradation. Mechanical contact is one

of the major factors that are responsible for the damage of FGMs. SURESH *et al.* were the first to perform an indentation experiment aiming to measure the contact damages of FGMs resulting from impact loading and surface invasion [2]. A number of mechanical properties can be predicted from the experiments of this kind. Later, SURESH *et al.* further concluded that the damage and failure resistance of a solid surface to both quasistatic and dynamic contact loading can be substantially improved by using FGMs [3].

In the experimental and theoretical study of contact mechanics involving FGMs, simple mathematical functions, such as exponential and power law distributions, are typically chosen to represent the spatial gradient of shear modulus. For most engineering materials, the Poisson's ratio does not vary much. Guler and Erdogan revisited the Hertzian contact problem between two deformable elastic solids with exponentially graded elastic coating [4]. The same authors also solved the frictional sliding contact problem between a rigid stamp and a homogeneous substrate with graded coating [5]. ELLOUMI *et al.* studied the non-linear partial slip contact problem of an exponentially graded half-plane indented by a rigid punch [6]. Following this line of research, GULER *et al.* have recently investigated the plane contact problem of an exponentially graded elastic half-plane in sliding contact with a rigid punch [7].

Contact problems associated with FGMs assuming a power-law distribution of elastic modulus have also received much attention. In a single study, Giannakopoulos and Pallot tackled the normal, sliding and rolling type of contact of a rigid cylinder on a graded elastic substrate [8]. The adhesive contact problem between a rigid sphere and a power-law graded elastic half-space has also been solved [9].

Both the exponential and power-law model suggest a continuous and sufficiently smooth distribution of elastic modulus. A multilayered model that divides an FGM layer into several sublayers has been developed to address a possible demand for less smoother grading of elastic modulus. In this model, the shear modulus is assumed to vary linearly within each sublayer and is continuous at every interface among the sublayers [10]. In the framework of the multilayered model, KE and WANG solved the frictionless contact problem of an FGM coated half-plane indented by flat, triangular and cylindrical stamps [11]. LIU *et al.* further extended the multilayered model to examining axisymmetric contact problems [12].

All the literature reviewed above focuses on the advancing and stationary contact problems. Problems concerning receding contact form another important branch of contact mechanics [13]. As a simple example, let us consider an air mattress resting on the floor. Due to gravity, the mattress can be assumed to be in full contact with the floor. A receding contact occurs after a child jumps onto the mattress, formed from the shrinking area of contact during the loading

process. Nowadays, decks of battleships are often coated with FGMs, which help to prevent the decks from wear and damage due to a high strain rate typically occurring during taking-off and landing of aircrafts. Receding contact inevitably occurs in individual laminates in a multilayered deck structure.

Due to the limited area of receding contact, significant stresses develop in and nearby the contact region, making the material highly susceptible to damage and failure. Nevertheless, few studies have focused on receding contact problems. Even less research was devoted to the receding contact of FGMs. El-Borgi *et al.* investigated both the frictionless and the frictional receding contact mechanics between an FGM layer and an elastic substrate [14, 15]. The frictionless version was shortly generalized to the axisymmetric case by RHIMI *et al.* [16]. In addition, ADIYAMAN considered an FGM layer supported by two homogeneous quarter planes [17]. These above mentioned studies are all concerned with single receding contact, since, instead of using an indenter, traction loads are directly applied onto the other surface of the FGM layer.

By replacing the normal pressure with an axisymmetric rigid stamp, RHIMI *et al.* solved the double contact problem of an FGM layer [18]. In the same way, YAN *et al.* further explored the double contact problem of an FGM layer pressed against an elastic substrate of finite thickness by a rigid circular punch [19]. Furthermore, Çömez has recently solved the receding contact problem between two FGM media, both of finite thickness. In addition to the exponential model universally used in the receding contact problems stated above, LIU *et al.* investigated the axisymmetric receding contact problem of an FGM layer indented against a homogeneous substrate, by the use of the multilayered model [20].

Previous work on the mechanics of receding contact addressed at most two layers, i.e., models formed by the combination of two elements out of an elastic strip, an FGM layer, or a half-plane substrate. Multilayered laminates constructed by distinct layers perfectly bonded together, however, are one common component employed in engineering structures [21, 22]. A number of fundamental issues in the receding contact of these models, particularly in those involving an FGM element, remain unresolved [23, 24]. As one step to this end, we consider in this paper a double contact problem composed of three layers: a homogeneous elastic strip, an FGM layer, and a half-plane substrate. The elastic strip and the FGM layer are assumed to be perfectly bonded along their interface, neglecting any possible mismatch strains.

The three-layer system is then loaded by a rigid punch with a convex perimeter, resulting in both an advancing contact at the indenter-elastic strip interface and a receding contact between the FGM-substrate interface. We assume frictionless conditions at both contact interfaces. The distribution of the shear modulus of the FGM layer is modeled by an exponential function, varying along its thickness. By employing the method of Fourier integral transforms,

the equations of equilibrium of the double contact problem are transformed into a pair of singular integral equations. Extensive numerical calculations are subsequently performed to illustrate the impact of indentation load, geometric dimensions and material properties of individual components on the contact pressure and the contact length at both contact interfaces. Although the numerical experiments were performed with reference to a rigid circular punch, the proposed mathematical formulation is equally valid for convex punches of other shapes.

The remainder of this paper is organized as follows. Section 2 outlines the mathematical formulation of the proposed double contact problem. The main result of this section is a pair of singular integral equations whose solution algorithm is detailed in Section 3. In Section 4, a variety of numerical experiments detailing the contact pressure and the contact length at both contact interfaces are reported and discussed. Finally, in Section 5, conclusions are provided and future works described.

2. Formulation of the double contact problem

As shown in Fig. 1, let us consider a rigid circular indenter of radius R pressed against a two-layer composite, which is composed of a homogeneous elastic strip of thickness h_1 and an FGM layer of thickness h_2 . These two media are perfectly bonded at their interface and supported as a whole by a homogeneous half-plane substrate. Both the elastic strip and the half-plane substrate are homogeneous, characterized by their shear moduli μ_1 and μ_3 , whereas the mechanical property

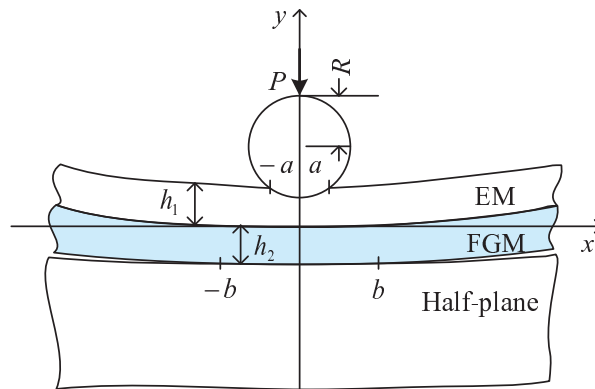


FIG. 1. Schematic of the double contact problem consisting of an advancing contact between a rigid circular punch and an elastic strip and a receding contact between a functionally graded layer and a homogeneous half-plane. The elastic strip and the functionally graded layer are assumed to be perfectly bonded.

of the FGM layer is assumed to be position-dependent:

$$(2.1) \quad \mu_2(y) = \mu_1 e^{-\beta y}, \quad -h_2 \leq y < 0,$$

where β is an arbitrary nonzero constant. In the absence of body forces, the elastostatic Navier equations of equilibrium for the three deformable media are given by

$$(2.2a) \quad (\kappa+1) \frac{\partial^2 u_l}{\partial x^2} + (\kappa-1) \frac{\partial^2 u_l}{\partial y^2} + 2 \frac{\partial^2 v_l}{\partial x \partial y} = 0,$$

$$(2.2b) \quad (\kappa-1) \frac{\partial^2 v_l}{\partial x^2} + (\kappa+1) \frac{\partial^2 v_l}{\partial y^2} + 2 \frac{\partial^2 u_l}{\partial x \partial y} = 0,$$

$$(2.2c) \quad (\kappa+1) \frac{\partial^2 u_2}{\partial x^2} + (\kappa-1) \frac{\partial^2 u_2}{\partial y^2} + 2 \frac{\partial^2 v_2}{\partial x \partial y} - \beta(\kappa-1) \frac{\partial u_2}{\partial y} - \beta(\kappa-1) \frac{\partial v_2}{\partial x} = 0,$$

$$(2.2d) \quad (\kappa-1) \frac{\partial^2 v_2}{\partial x^2} + (\kappa+1) \frac{\partial^2 v_2}{\partial y^2} + 2 \frac{\partial^2 u_2}{\partial x \partial y} - \beta(3-\kappa) \frac{\partial u_2}{\partial x} - \beta(\kappa+1) \frac{\partial v_2}{\partial y} = 0,$$

where the parameter κ is related to Poisson's ratio ν , i.e., $\kappa = 3 - 4\nu$ for plane strain and $\kappa = (3 - \nu)/(1 + \nu)$ for plane stress. It should be clear that the first two equations of (2.2a) work for the homogeneous elastic strip and half-plane substrate ($l = 1$ or 3). The technique of standard Fourier transform is now applied to Eqs. (2.2a–d) since we prefer to work in the transformed space. For the homogeneous elastic strip ($0 \leq y \leq h_1$), the transformed displacements and stresses are given by

$$(2.3a) \quad \tilde{u}_1(\lambda, y) = (C_1 + yC_2)e^{\lambda y} + (C_3 + yC_4)e^{-\lambda y},$$

$$(2.3b) \quad \tilde{v}_1(\lambda, y) = i \left[\left(C_1 + \left(y - \frac{\kappa}{\lambda} \right) C_2 \right) e^{\lambda y} - \left(C_3 + \left(y + \frac{\kappa}{\lambda} \right) C_4 \right) e^{-\lambda y} \right];$$

$$(2.4a) \quad \begin{aligned} \tilde{\sigma}_{yy1}(\lambda, y) = 2\mu_1 i \left[\left(\lambda C_1 - \left(\frac{1+\kappa}{2} - \lambda y \right) C_2 \right) e^{\lambda y} \right. \\ \left. + \left(\lambda C_3 + \left(\frac{1+\kappa}{2} + \lambda y \right) C_4 \right) e^{-\lambda y} \right], \end{aligned}$$

$$(2.4b) \quad \begin{aligned} \tilde{\sigma}_{xy1}(\lambda, y) = 2\mu_1 \left[\left(\lambda C_1 + \left(\frac{1-\kappa}{2} + \lambda y \right) C_2 \right) e^{\lambda y} \right. \\ \left. - \left(\lambda C_3 - \left(\frac{1-\kappa}{2} - \lambda y \right) C_4 \right) e^{-\lambda y} \right], \end{aligned}$$

where C_1, C_2, C_3 and C_4 are unknown functions of the transformation variable λ , to be determined from the boundary conditions of the present problem. In a similar fashion, the displacements and stresses for the FGM layer ($-h_2 \leq y < 0$) in

the Fourier transformed space can be derived as

$$(2.5a) \quad \tilde{u}_2(\lambda, y) = \sum_{k=1}^4 C_{k+4} e^{m_k y},$$

$$(2.5b) \quad \tilde{v}_2(\lambda, y) = \sum_{k=1}^4 C_{k+4} s_k e^{m_k y};$$

$$(2.6a) \quad \tilde{\sigma}_{yy2}(\lambda, y) = \frac{\mu_1 e^{-\beta y}}{\kappa - 1} \sum_{k=1}^4 [-i\lambda(3 - \kappa) + (1 + \kappa)m_k s_k] C_{k+4} e^{m_k y},$$

$$(2.6b) \quad \tilde{\sigma}_{xy2}(\lambda, y) = \mu_1 e^{-\beta y} \sum_{k=1}^4 [m_k - i\lambda s_k] C_{k+4} e^{m_k y},$$

where

$$(2.7a) \quad m_1(\lambda) = \frac{1}{2} \left(\beta + \sqrt{\beta^2 + 4\lambda^2 - 4i\beta\lambda \sqrt{\frac{3-\kappa}{1+\kappa}}} \right),$$

$$(2.7b) \quad m_2(\lambda) = \frac{1}{2} \left(\beta - \sqrt{\beta^2 + 4\lambda^2 - 4i\beta\lambda \sqrt{\frac{3-\kappa}{1+\kappa}}} \right),$$

$$(2.7c, d) \quad m_3(\lambda) = \bar{m}_1(\lambda), \quad m_4(\lambda) = \bar{m}_2(\lambda),$$

$$(2.8) \quad s_k(\lambda) = \frac{(\kappa - 1)m_k^2 - \beta(\kappa - 1)m_k - \lambda^2(\kappa + 1)}{i\lambda(2m_k - \beta(\kappa - 1))}, \quad k = 1, 2, 3, 4,$$

and C_5 , C_6 , C_7 and C_8 are also unknown functions of λ . They can also be determined by enforcing the boundary conditions. Due to the semiinfinite nature of the half-plane substrate ($-\infty < y < -h_2$), it is easy to see

$$(2.9a, b) \quad u_3(x, y) = 0, \quad v_3(x, y) = 0, \quad x^2 + y^2 \rightarrow \infty.$$

In view of the above equations (2.9a, b), the displacements and stresses of the half-plane substrate in the transformed space can be significantly simplified

$$(2.10a) \quad \tilde{u}_3(\lambda, y) = (C_9 + C_{10}y)e^{|\lambda|y},$$

$$(2.10b) \quad \tilde{v}_3(\lambda, y) = i \left[C_9 \frac{\lambda}{|\lambda|} + \left(\frac{\lambda}{|\lambda|} y - \frac{\kappa}{\lambda} \right) C_{10} \right] e^{|\lambda|y};$$

$$(2.11a) \quad \tilde{\sigma}_{yy3}(\lambda, y) = 2i\mu_3 \left[\lambda C_9 + \left(-\frac{(1+\kappa)\lambda}{2|\lambda|} + \lambda y \right) C_{10} \right] e^{|\lambda|y},$$

$$(2.11b) \quad \tilde{\sigma}_{xy3}(\lambda, y) = 2\mu_3 \left[|\lambda| C_9 + \left(\frac{1-\kappa}{2} + |\lambda|y \right) C_{10} \right] e^{|\lambda|y}.$$

It is seen that only two unknown functions, i.e., C_9 and C_{10} , are required to determine the elastic fields in the substrate.

For the frictionless contact, the boundary conditions at the indenter-elastic strip interface ($y = h_1$) are straightforward:

$$(2.12a, b) \quad \sigma_{yy1}(x, h_1) = -p(x)H(a - |x|), \quad \sigma_{xy1}(x, h_1) = 0, \quad |x| < \infty,$$

where $H(a - |x|)$ denotes the Heaviside step function and a is the half contact length. It should be noted that here we have chosen to formulate the boundary conditions at the advancing contact interface in terms of contact pressure $p(x)$. Later, this unknown function will be related to the displacement boundary conditions at the same interface.

Since the elastic strip and the FGM layer are assumed to be perfectly bonded, both displacements and stresses must be continuous across their interface ($y = 0$)

$$(2.13a, b) \quad \sigma_{yy1}(x, 0) = \sigma_{yy2}(x, 0), \quad \sigma_{xy1}(x, 0) = \sigma_{xy2}(x, 0), \quad |x| < \infty,$$

$$(2.13c, d) \quad u_1(x, 0) = u_2(x, 0), \quad v_1(x, 0) = v_2(x, 0), \quad |x| < \infty.$$

For the receding contact occurring at the FGM-substrate interface ($y = -h_2$), the frictionless assumption yields

$$(2.14a, b) \quad \sigma_{yy2}(x, -h_2) = -q(x)H(b - |x|), \quad \sigma_{xy2}(x, -h_2) = 0, \quad |x| < \infty,$$

$$(2.14c, d) \quad \sigma_{yy3}(x, -h_2) = -q(x)H(b - |x|), \quad \sigma_{xy3}(x, -h_2) = 0, \quad |x| < \infty,$$

where $q(x)$ is the contact pressure and b is the half contact length.

Alternatively, the normal component of the traction boundary conditions at both the advancing and the receding contact interface can be expressed in terms of displacements:

$$(2.15a) \quad \frac{\partial v_1(x, h_1)}{\partial x} = f(x), \quad |x| < a,$$

$$(2.15b) \quad \frac{\partial v_2(x, -h_2)}{\partial x} = \frac{\partial v_3(x, -h_2)}{\partial x}, \quad |x| < b,$$

where $f(x)$ stands for the slope of the stamp profile. To eliminate possible rigid body displacements, these two equations were deliberately formulated with respect to the slopes of both contact interfaces. Furthermore, it is worth noting that at both the advancing and the receding contact interface integration of contact pressure must balance the indentation load (P) applied to the rigid stamp

$$(2.16a, b) \quad \int_{-a}^a p(t)dt = P, \quad \int_{-b}^b q(t)dt = P.$$

The above three groups of boundary conditions (2.12a, b; 2.13a–d; 2.14a–d) provide ten equations to evaluate the ten unknown functions $C_k(\lambda)$, $k = 1, \dots, 10$, in terms of contact pressures and half contact lengths. This process is accomplished by substituting the displacements and stresses in the transformed space, i.e. Eqs. (2.3a, b; 2.4a, b; 2.5a, b; 2.6a, b; 2.11a, b), into the Fourier transforms of the boundary conditions

$$(2.17a) \quad C_k = (-1)^k \left(\frac{D_{1k}}{D} \tilde{P} + \frac{D_{7k}}{D} \tilde{Q} \right), \quad k = 1, \dots, 8,$$

$$(2.17b, c) \quad C_9 = \frac{(2|\lambda|h_2 - 1 + \kappa)\mu_1 e^{(|\lambda|+\beta)h_2}}{4i\lambda\mu_3(\kappa - 1)} \tilde{Q}, \quad C_{10} = \frac{|\lambda|\mu_1 e^{(|\lambda|+\beta)h_2}}{2i\lambda\mu_3(\kappa - 1)} \tilde{Q},$$

where

$$(2.18a, b) \quad \tilde{P}(\lambda) = \frac{1}{2\pi\mu_1} \int_{-a}^a p(t) e^{it\lambda} dt, \quad \tilde{Q}(\lambda) = \frac{\kappa - 1}{2\pi\mu_1 e^{\beta h_2}} \int_{-b}^b q(t) e^{it\lambda} dt,$$

and D_{jk} denotes the determinant of a 7×7 matrix obtained by eliminating the j th row and k th column of an 8×8 square matrix D . The expression for this matrix is detailed in the Appendix. It is noted that the pressure functions ($p(x)$ and $q(x)$) and the half contact lengths (a and b) are still unknowns that must be eventually determined from Eqs. (2.15a, b) and (2.16a, b). Substituting Eqs. (2.17a–c) back into the vertical displacement components (2.3b), (2.5b), and (2.10b), and subsequently implementing the displacement boundary conditions (2.15a, b), we arrive at a pair of singular integral equations

$$(2.19a) \quad \frac{1}{\pi\mu_1} \int_{-a}^a k_1(x, t) p(t) dt + \frac{\kappa - 1}{\pi\mu_1 e^{\beta h_2}} \int_{-b}^b k_2(x, t) q(t) dt = f(x), \quad |x| \leq a,$$

$$(2.19b) \quad \int_{-a}^a k_3(x, t) p(t) dt + \frac{\kappa - 1}{e^{\beta h_2}} \int_{-b}^b k_4(x, t) q(t) dt = 0, \quad |x| \leq b,$$

where

$$(2.20a) \quad k_1(x, t) = \int_0^\infty A(\lambda) \sin[\lambda(t - x)] d\lambda,$$

$$(2.20b) \quad k_2 = \int_0^{+\infty} i \left[\left(-\lambda \frac{D_{71}}{D} + (\lambda h_1 - \kappa) \frac{D_{72}}{D} \right) e^{\lambda h_1} - \left(-\lambda \frac{D_{73}}{D} + (\lambda h_1 + \kappa) \frac{D_{74}}{D} \right) e^{-\lambda h_1} \right] \sin[\lambda(t - x)] d\lambda,$$

$$(2.20c) \quad k_3 = \int_0^{+\infty} \lambda \left[\sum_{k=1}^4 (-1)^k \frac{D_{1k+4}}{D} s_k e^{-m_k h_2} \right] \sin[\lambda(t-x)] d\lambda,$$

$$(2.20d) \quad k_4(x, t) = \int_0^{\infty} B(\lambda) \sin[\lambda(t-x)] d\lambda,$$

in which

$$(2.21a) \quad A(\lambda) = i \left(-\lambda \frac{D_{11}}{D} + (\lambda h_1 - \kappa) \frac{D_{12}}{D} \right) e^{\lambda h_1} \\ - i \left(-\lambda \frac{D_{13}}{D} + (\lambda h_1 + \kappa) \frac{D_{14}}{D} \right) e^{-\lambda h_1},$$

$$(2.21b) \quad B(\lambda) = \lambda \left[\sum_{k=1}^4 (-1)^k \frac{D_{7k+4}}{D} s_k e^{-m_k h_2} \right] + \frac{\mu_1(1+\kappa)e^{\beta h_2}}{4\mu_3(\kappa-1)}.$$

Asymptotic analysis helps to greatly simplify Eqs. (2.21a, b) [25]

$$(2.22a, b) \quad A(\lambda) = a_0 + \mathcal{O}\left(\frac{1}{\lambda}\right), \quad B(\lambda) = b_0 + \mathcal{O}\left(\frac{1}{\lambda}\right),$$

where

$$(2.23a, b) \quad a_0 = -\frac{1+\kappa}{4}, \quad b_0 = \frac{(1+\kappa)(e^{\beta h_2} \mu_1 + \mu_3)}{4\mu_3(\kappa-1)}.$$

By the use of these results, Eqs. (2.19a, b) now become

$$(2.24a) \quad \int_{-a}^a \left[\frac{1}{t-x} + k_5(x, t) \right] p(t) dt + \frac{\kappa-1}{a_0 e^{\beta h_2}} \int_{-b}^b k_2(x, t) q(t) dt = \frac{\pi \mu_1}{a_0} f(x), \quad |x| \leq a,$$

$$(2.24b) \quad \frac{e^{\beta h_2}}{b_0(\kappa-1)} \int_{-a}^a k_3(x, t) p(t) dt + \int_{-b}^b \left[\frac{1}{t-x} + k_6(x, t) \right] q(t) dt = 0, \quad |x| \leq b,$$

where

$$(2.25a) \quad k_5(x, t) = \int_0^{\infty} \left[\frac{A(\lambda)}{a_0} - 1 \right] \sin[\lambda(t-x)] d\lambda,$$

$$(2.25b) \quad k_6(x, t) = \int_0^{\infty} \left[\frac{B(\lambda)}{b_0} - 1 \right] \sin[\lambda(t-x)] d\lambda.$$

3. Solution to dual singular integral equations

In this section, we aim to develop an efficient and robust algorithm to numerically tackle the fundamental unknowns of the present double contact problem, i.e., $p(x)$, $q(x)$, a , and b . To this end, let us first define a few dimensionless variables

$$(3.1a-d) \quad r_1 = \frac{x}{a}, \quad r_2 = \frac{x}{b}, \quad s_1 = \frac{t}{a}, \quad s_2 = \frac{t}{b},$$

$$(3.1e, f) \quad p_1(s_1) = \frac{p(t)}{P/h_1}, \quad q_1(s_2) = \frac{q(t)}{p/h_1},$$

$$(3.1g, h) \quad k_2(x, t) = K_2(r_1, s_2), \quad k_3(x, t) = K_3(r_2, s_1),$$

$$(3.1j, k) \quad k_5(x, t) = K_5(r_1, s_1), \quad k_6(x, t) = K_6(r_2, s_2).$$

The dual singular integral equations (2.24a, b) and the force equilibrium conditions (2.16a, b) can therefore be nondimensionalized:

$$(3.2a) \quad \int_{-1}^1 \left[\frac{1}{s_1 - r_1} + aK_5(r_1, s_1) \right] p_1(s_1) ds_1 \\ + \frac{b(\kappa - 1)}{a_0 e^{\beta h_2}} \int_{-1}^1 K_2(r_1, s_2) q_1(s_2) ds_2 = \frac{\pi \mu_1}{a_0 P/h_1} f(r_1), \quad |r_1| \leq 1,$$

$$(3.2b) \quad \frac{a e^{\beta h_2}}{b_0(\kappa - 1)} \int_{-1}^1 K_3(r_2, s_1) p_1(s_1) ds_1 \\ + \int_{-1}^1 \left[\frac{1}{s_2 - r_2} + bK_6(r_2, s_2) \right] q_1(s_2) ds_2 = 0, \quad |r_2| \leq 1,$$

$$(3.2c, d) \quad \frac{a}{h_1} \int_{-1}^1 p_1(s_1) ds_1 = 1, \quad \frac{b}{h_1} \int_{-1}^1 q_1(s_2) ds_2 = 1.$$

Given the fact that all four dimensionless independent variables, i.e., r_1 , r_2 , s_1 , and s_2 share the same closed interval $[-1, 1]$, their subscripts can be safely dropped. One of the quadrature rules applicable to Eqs. (3.2a–d) is Chebyshev–Gauss formula [26, 27]. Consequently, an N -point quadrature rule discretizes Eqs. (3.2a–d) to

$$(3.3a) \quad \sum_{k=1}^N \frac{1 - s_k^2}{N + 1} \left\{ \left[\frac{1}{s_k - r_j} + aK_5(r_j, s_k) \right] P(s_k) \right. \\ \left. + \frac{b(\kappa - 1)}{a_0 e^{\beta h_2}} K_2(r_j, s_k) Q(s_k) \right\} = \frac{\mu_1}{a_0 P/h_1} f(r_j),$$

$$(3.3b) \quad \sum_{k=1}^N \frac{1-s_k^2}{N+1} \left\{ \frac{ae^{\beta h_2}}{b_0(\kappa-1)} K_3(r_j, s_k) P(s_k) \right. \\ \left. + \left[\frac{1}{s_k - r_j} + bK_6(r_j, s_k) \right] Q(s_k) \right\} = 0,$$

$$(3.3c, d) \quad \frac{\pi a}{h_1} \sum_{k=1}^N \frac{1-s_k^2}{N+1} P(s_k) = 1, \quad \frac{\pi b}{h_1} \sum_{k=1}^N \frac{1-s_k^2}{N+1} Q(s_k) = 1,$$

where

$$(3.4a) \quad s_k = \cos\left(\frac{k\pi}{N+1}\right), \quad k = 1, \dots, N,$$

$$(3.4b) \quad r_j = \cos\left(\frac{\pi(2j-1)}{2(N+1)}\right), \quad j = 1, \dots, N+1,$$

$$(3.4c) \quad P(s) = p_1(s)(1-s^2)^{-1/2},$$

$$(3.4d) \quad Q(s) = q_1(s)(1-s^2)^{-1/2}, \quad |s| \leq 1.$$

Without loss of generality, we may choose N as an even number. In this case, Eqs. (3.3a,b) are automatically satisfied for $j = N/2 + 1$ [26]. As a result, Eqs. (3.3a–d) render us a total number of $2N + 2$ algebraic equations for the same number of unknowns, i.e., $P(s_k)$, $Q(s_k)$, a and b . This system of equations is simply linear for $P(s_k)$ and $Q(s_k)$, but highly nonlinear for the half contact lengths a and b . A numerical algorithm for the calculation of these unknown functions can be summarized as follows.

1. Make initial guesses at the half contact lengths a and b .
2. Calculate functions $P(s_k)$ and $Q(s_k)$, by Eqs. (3.3a, b).
3. Evaluate the residual errors of Eqs. (3.3c, d). If both residuals are found to be less than a predefined degree of tolerance, e.g. 10^{-5} , the calculation can be satisfactorily terminated. Otherwise, guesses of a and b must be updated by following the method of steepest descent (the Newton downhill method) [28].

4. Results and discussion

While the solution strategy developed in the previous sections is valid for arbitrary rigid punches of convex profiles, in this section we discuss parametric studies due to a rigid circular punch of radius R . The slope function of such a simple punch is given by

$$(4.1) \quad f(x) = x(R^2 - x^2)^{-1/2}, \quad |x| \leq a.$$

To calibrate the accuracy and robustness of the developed algorithm, we first tested a simplified version of the model shown in Fig. 1 by assigning $h_2 = 0$. In this case, the original geometry degenerates to an elastic layer pressed against a homogeneous half-plane by a rigid circular punch. Table 1 compares the half lengths at both the advancing and the receding contact interface obtained in the present study with those presented in KAHYA *et al.* [29], for several combinations of stamp size and indentation load. To make these results comparable, all parameters and variables were nondimensionalized. Although marginal, the improved residual errors of Eqs. (3.3c, d) clearly demonstrate the accuracy of the developed algorithm.

Table 1. Comparison of the half contact lengths obtained in the present study with those reported in the literature [29] for a few combinations of stamp radius and indentation load. Also tabulated in the table are the residual errors of the forces transmitted across both the advancing (E_{adv}) and the receding (E_{rec}) contact interface, cf. Eqs. (3.3c, d).

R/h_1	$\mu_1 h_1/P$	a/h_1		E_{adv}		b/h_1		E_{rec}	
		Present	Kahya	Present	Kahya	Present	Kahya	Present	Kahya
10	500	0.0979	0.0979	3.48E-08	5.85E-05	1.3271	1.3300	9.78E-06	9.60E-05
	1000	0.0692	0.0692	9.89E-06	1.87E-05	1.3248	1.3250	8.46E-06	1.87E-05
	2000	0.0489	0.0489	2.93E-06	7.81E-05	1.3298	1.3300	9.98E-06	9.13E-05
500	500	0.7422	0.7426	1.56E-06	5.75E-05	1.5028	1.5026	9.88E-06	1.08E-05
	1000	0.5110	0.5111	9.54E-06	9.06E-05	1.3980	1.3980	5.62E-06	7.79E-05
	2000	0.3542	0.3543	9.52E-06	9.42E-05	1.3557	1.3557	4.06E-06	6.54E-05

Table 2. Variation of the half contact lengths at both the advancing and the receding contact interface as functions of normalized stamp radius, indentation force, and FGM layer stiffness for the simplified model shown in Fig. 2.

R/h_2	$\mu_3 h_2/P$	$\beta h_2 = -1$		$\beta h_2 = 0.001$		$\beta h_2 = 1$	
		a/h_2	b/h_2	a/h_2	b/h_2	a/h_2	b/h_2
10	100	0.2444	1.1650	0.2208	1.3328	0.2041	1.5844
	500	0.1028	1.1478	0.0979	1.3300	0.0940	1.5820
	1000	0.0716	1.1422	0.0692	1.3248	0.0671	1.5774
250	100	1.4186	1.7669	1.2171	1.7621	1.0628	1.8713
	500	0.6029	1.2746	0.5106	1.4198	0.4480	1.6402
	1000	0.4080	1.2040	0.3542	1.3543	0.3178	1.6048
500	100	1.9834	2.2332	1.7418	2.1596	1.5560	2.2334
	500	0.8815	1.4190	0.7424	1.5020	0.6419	1.6825
	1000	0.6029	1.2747	0.5110	1.3978	0.4479	1.3554

As an alternative to the simplified model studied in [29], we further considered the degenerated case of the receding contact problem between an FGM layer and a half-plane substrate, as sketched in Fig. 2. In this model, the elastic strip was simply removed ($h_1 = 0$). The effects of stamp radius, thickness of the FGM layer, and substrate stiffness on the half contact lengths at both the advancing and the receding contact interface are numerically investigated, for three types of FGM models. Table 2 tabulates the contact sizes at both the stamp-FGM and FGM-substrate interface for 27 combinations of the above mentioned governing parameters. It can be seen that larger stamps always lead to higher values of contact lengths at both interfaces. For punches with the same size, larger indentation forces result in more intensive contact among three components of the structure. Both observations are universally true, irrespective of the stiffness of the FGM layer.

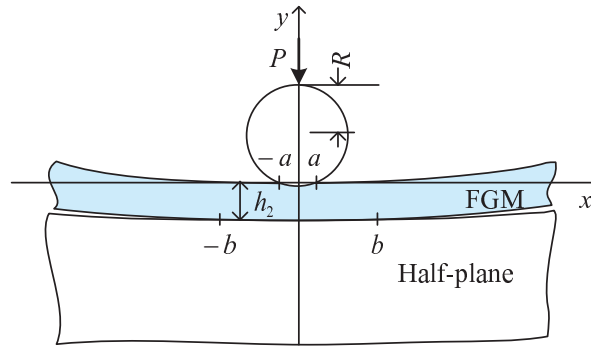


FIG. 2. A functionally graded layer pressed against an elastic half-plane by a rigid circular stamp. This setting represents a simplified model in comparison to the one shown in Fig. 1.

In the remainder of this section, we aim to numerically investigate the contact pressure and the contact size at both interfaces for the full model shown in Fig. 1. Figs. 3 and 4 present the distributions of the advancing and the receding contact pressure for three values of the FGM layer stiffness, respectively. To concentrate on the influence of the FGM layer stiffness, the remaining parameters are all chosen as constants, i.e. $h_1 = h_2$, $\mu_1 = \mu_3$, $\mu_1 h_1 / P = 500$ and $R / h_1 = 1000$. At both contact interfaces, it is evident that the maximum contact pressure and the contact length are negatively correlated. In addition, both pressure distributions conform according to our intuition. Under the application of a concentrated load, distributions of both contact pressures are symmetric about the vertical axis passing through the center of the circular stamp. At either of the contact interfaces, the maximum pressure is identified at the center of stamp tip.

As explained by Eq. (2.1), a positive βh_2 represents a hard FGM layer whereas a negative βh_2 stands for a soft one. The special case of a homoge-

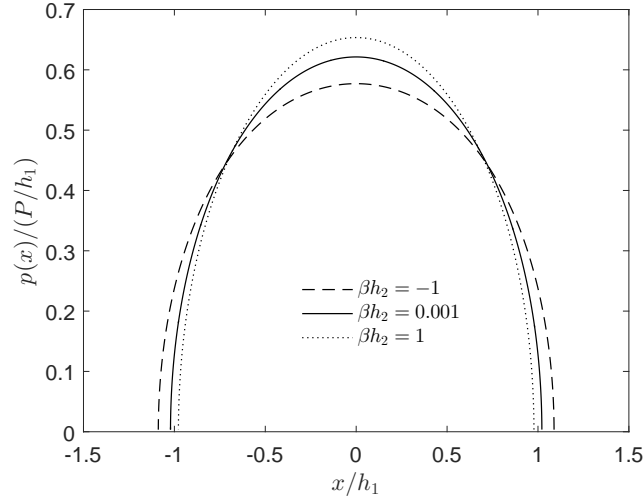


FIG. 3. Distribution of the advancing contact pressure $p(x)$ along the stamp-elastic strip interface. The adjustable parameters are set to: $h_1 = h_2$, $\mu_1 = \mu_3$, $\mu_1 h_1 / P = 500$ and $R/h_1 = 1000$.

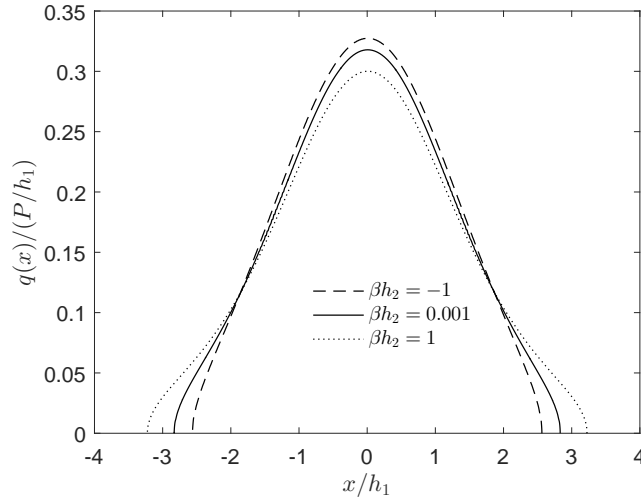


FIG. 4. Distribution of the receding contact pressure $q(x)$ along the FGM-substrate interface. The adjustable parameters assume the same values as their counterparts used to produce Fig. 3.

neous elastic strip can reasonably be approximated by assigning the FGM layer stiffness $\beta h_2 = 0.001$. This setting, again, degenerates to the simplified model of an elastic layer of thickness $h_1 + h_2$ indented against a half-plane substrate by

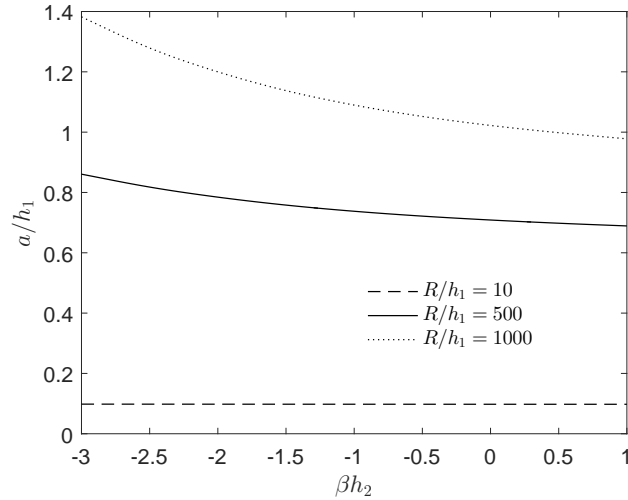


FIG. 5. Variation of the half contact length at the advancing contact interface as a function of the FGM layer stiffness. The adjustable parameters are chosen as: $h_1 = h_2$, $\mu_1 = \mu_3$ and $\mu_1 h_1/P = 500$.

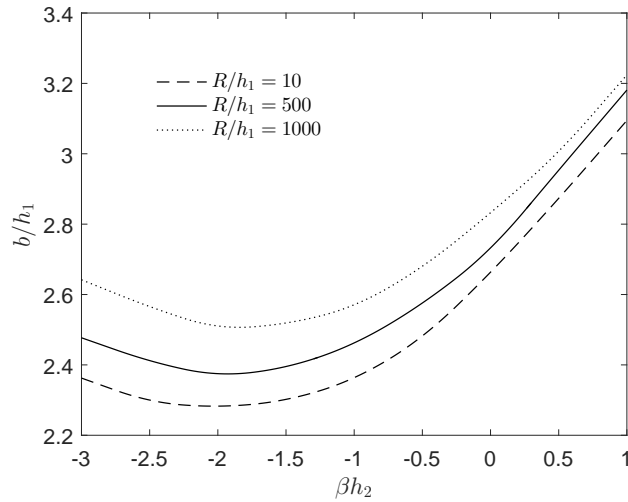


FIG. 6. Variation of the half contact length at the receding contact interface as a function of the FGM layer stiffness. The adjustable parameters assume the same values as their counterparts used to produce Fig. 5.

a rigid punch. Such a neutral FGM layer provides us with a basis for comparison. It is found that the maximum contact pressure at the advancing contact interface is always larger than that at the receding contact interface, regardless

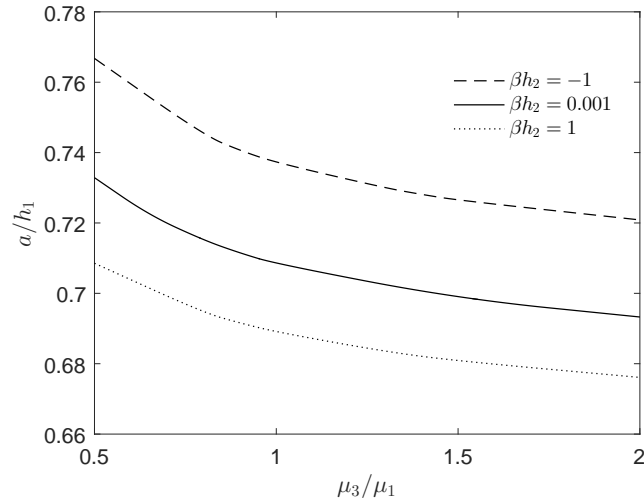


FIG. 7. Variation of the half contact length at the advancing contact interface as a function of the shear moduli ratio μ_3/μ_1 . The adjustable parameters are chosen as: h_1/h_2 , $R/h_1 = 500$ and $\mu_1 h_1/P = 500$.

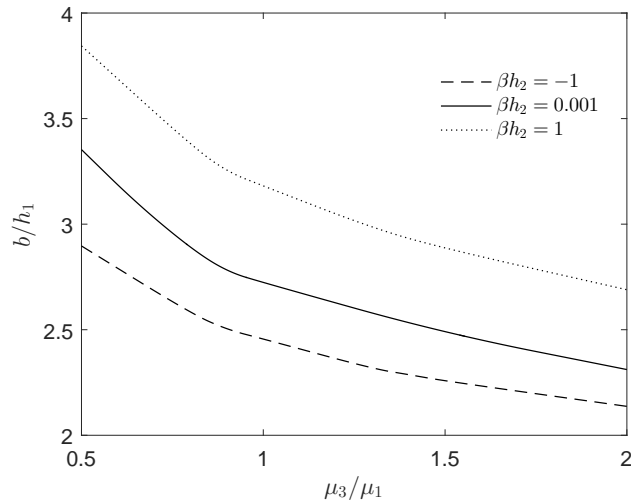


FIG. 8. Variation of the half contact length at the receding contact interface as a function of the shear moduli ratio μ_3/μ_1 . The adjustable parameters assume the same values as their counterparts used to produce Fig. 7.

of the FGM layer stiffness. On the contrary, longer contact length can always be found at the FGM-substrate interface, for all three values of the FGM layer stiffness.

Our next task is to explore the effects of the FGM layer stiffness on the contact length at both contact interfaces, as shown in Figs. 5 and 6. Three indenters of different sizes are considered. Both the contact size and the indenter radius are normalized with reference to the thickness of the elastic strip. While the FGM layer stiffness is allowed to vary, the values of other parameters are set to $h_2 = h_1$, $\mu_1 = \mu_3$ and $\mu_1 h_1 / P = 500$. As can be seen from Figs. 5 and 6, both contact lengths are increasing functions of the indenter radius, for all FGM layer stiffness considered in the numerical calculation ($-3 \leq \beta h_2 \leq 1$). This seems to be consistent with common sense.

Nonetheless, the ‘story’ is quite different for the functional dependence of the contact size on the FGM layer stiffness. At the advancing contact interface, the half contact length a monotonically decreases with the FGM layer stiffness. For the receding contact, a point of inflection is introduced, irrespective of the rigid punch size. The specific value of the FGM layer stiffness at which the receding contact size takes the minimum depends on the indenter radius. Large indenters tend to result in high values of the critical FGM layer stiffness. Let us recall that a universal law states that the contact size is inversely proportional to the maximum contact pressure. Consequently, if the receding contact pressure is of the primary concern in engineering practice, the critical FGM layer stiffness should be avoided. More generally, this observation provides a means of optimizing the FGM layer stiffness and indenter radius.

Figs. 7 and 8 show the variation of the half contact length at both contact interfaces as functions of the shear moduli ratio μ_3 / μ_1 . Three types of FGM layer were considered in the calculation, including negative ($\beta h_2 = -1$), nearly zero ($\beta h_2 = 0.001$) and positive ($\beta h_2 = 1$) FGM layer stiffness. The remaining governing parameters are chosen as $h_1 = h_2$, $R/h_1 = 500$ and $\mu_1 h_1 / P = 500$. It is observed that the half contact lengths at both contact interfaces are decreasing functions of the shear moduli ratio between the substrate and the elastic strip. In other words, a hard substrate always leads to small contact size and thus high maximum contact pressure at both interfaces. Therefore, the contact stresses at both the advancing and the receding contact interface can be controlled to a certain extent by the use of a reasonably soft substrate.

The impact of the thickness ratio between the FGM layer and the elastic strip h_2/h_1 on the nondimensionalized half contact lengths is shown in Figs. 9 and 10. Three types of FGM layer with distinct stiffness were calculated for both contact interfaces, while the other parameters are fixed as constants, i.e. $\mu_1 = \mu_3$, $R/h_1 = 500$ and $\mu_1 h_1 / P = 500$. The advancing and the receding contact lengths are in general a decreasing and increasing function of the thickness ratio, respectively. Particularly, the half contact length at the receding contact interface behaves nearly a linear function of the thickness ratio, for small thickness ratios (h_2/h_1). The half contact length at the advancing contact interface, on the

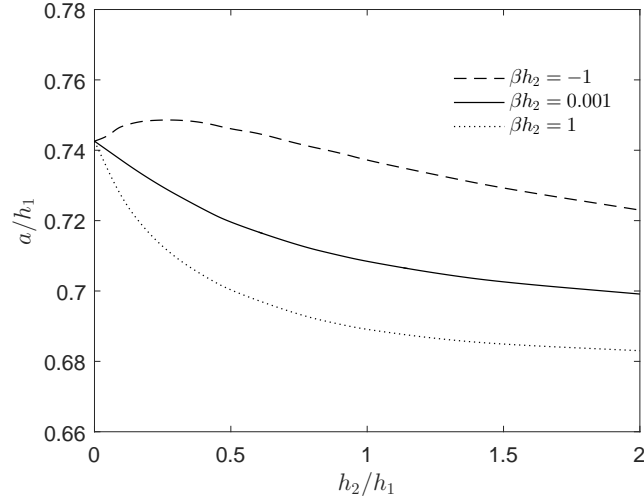


FIG. 9. Variation of the half contact length at the advancing contact interface as a function of the thickness ratio h_2/h_1 . The adjustable parameters are chosen as: $\mu_1 = \mu_3$, $R/h_1 = 500$ and $\mu_1 h_1/P = 500$.

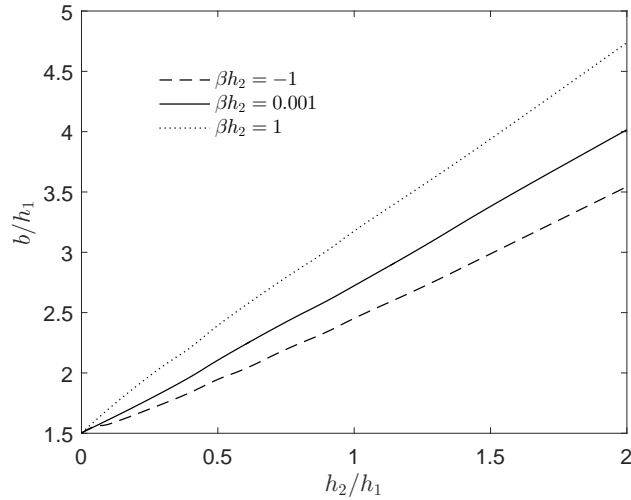


FIG. 10. Variation of the half contact length at the receding contact interface as a function of the thickness ratio h_2/h_1 . The adjustable parameters assume the same values as their counterparts used to produce Fig. 9.

other hand, shows strong nonlinearity. As can be inferred from the inverse proportionality between contact pressure and contact size, the greater the thickness ratio h_2/h_1 is the higher (lower) the maximum contact pressure develops at the

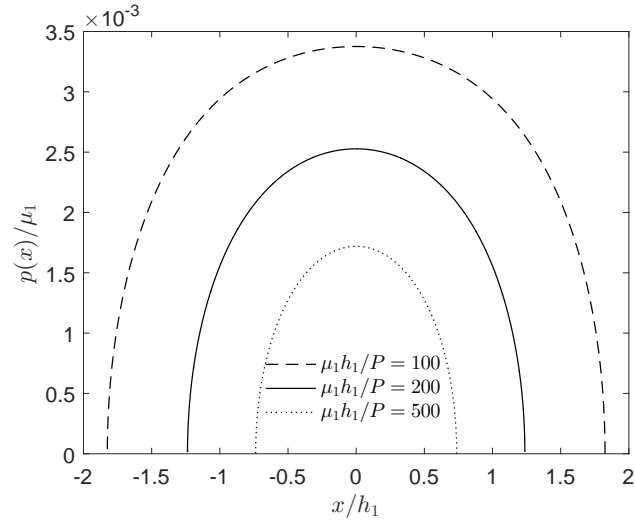


FIG. 11. Distribution of the advancing contact pressure $p(x)$ along the stamp-elastic strip interface. The adjustable parameters are set to: $\beta h_2 = -1$, $h_1 = h_2$, $\mu_1 = \mu_3$ and $R/h_1 = 500$.

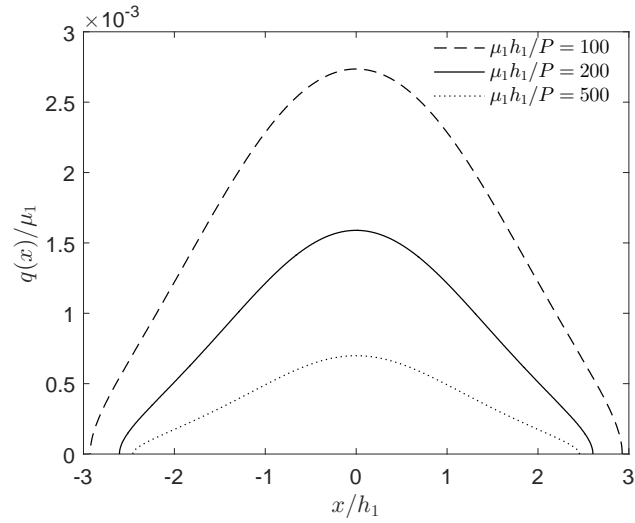


FIG. 12. Distribution of the receding contact pressure $q(x)$ along the FGM-substrate interface. The adjustable parameters assume the same values as their counterparts used to produce Fig. 11.

advancing (receding) contact interface. For the limiting case of a very thin FGM layer ($h_2 \rightarrow 0$), the contact pressure and the contact length at both interfaces converge to the degenerated case of a single elastic strip, cf. Table 1.

The last numerical experiment we performed aims to investigate the significance of the indentation load. Figs. 11 and 12 illustrate the distributions of the normalized advancing and receding contact stress. Three levels of normalized indentation forces are considered. In the meantime, the other governing parameters, such as the stiffness distribution of all deformable media, the thickness ratio of the elastic strip to the FGM layer, and the indenter radius, are all kept constant. It is observed that the magnitude of the indentation load serves as the most important factor in the determination of the results. Unlike the other factors, the qualitative effects of the indentation load on the contact pressure and contact size are identical. High indentation loads result in both high contact pressure and large contact size, at both the advancing and the receding contact interface. In Figs. 11 and 12, this conclusion is reflected by the fact that no intersections were found among the three curves of either plot.

5. Concluding remarks

In this paper, we successfully developed a semianalytical solution to the frictionless double contact problem of a double-layered laminate, pressed against a homogeneous elastic substrate by a rigid punch. The punch can be of any shape with a convex profile. The laminate is composed of a homogeneous elastic strip and an FGM layer, perfectly bonded along their interface. By the use of the method of Fourier transform, the elastostatic Navier equations of equilibrium were transformed into a pair of singular integral equations, formulated in terms of the contact pressure and the contact size at both the advancing and the receding contact interface. The dual singular integral equations were then numerically tackled by Chebyshev–Gauss quadrature. On the basis of extensive parametric studies involving the indentation load, the indenter radius, the thickness of both the elastic strip and the FGM layer, and the stiffness distribution of all deformable media, a few observations and conclusions regarding contact pressure and contact size can be drawn as follows.

First, under the application of a constant indentation force, the maximum contact pressure behaves as a decreasing function of the contact length, at both the advancing and the receding contact interface. Second, large indenters and indentation loads tend to increase the half contact length at both contact interfaces. By contrast, high maximum pressure resulted from small indenters and high indentation forces. Furthermore, soft and thin FGM layers can effectively reduce the advancing contact pressure. When low contact stress is preferred at the receding contact interface, a hard and thick FGM layer should be considered. Finally, soft substrates result in large receding and small advancing contact length.

In light of these findings, we believe that it is possible to optimize contact pressure and contact size by introducing FGM components into multilayered

elastic structures. Future work could entail extending our model to an FGM layer applied to other sites of a multilayered elastic composite.

Acknowledgements

This work was supported by the National Natural Science Foundation of China [grant number 11472079 and 51578136], the Natural Science Foundation of Jiangsu Province [grant number BK20161411], and the Fundamental Research Funds for the Central Universities. J.Y. would also like to thank the support by the Scientific Research and Innovation Project for Graduate Students in Colleges and Universities of Jiangsu Province [grant number KYLX16_0184].

Appendix: Expression for the matrix D first appeared in Eq. (2.17)

$$D = \begin{vmatrix} D' & O \\ O & D'' \end{vmatrix},$$

where O denotes a 2×4 zero matrix and

$$D' = \begin{bmatrix} 2i\lambda e^{\lambda h_1} & -i(1 + \kappa - 2\lambda h_1)e^{\lambda h_1} & 2i\lambda e^{-\lambda h_1} & i(1 + \kappa + 2\lambda h_1)e^{-\lambda h_1} \\ 2\lambda e^{\lambda h_1} & (1 - \kappa + 2\lambda h_1)e^{\lambda h_1} & -2\lambda e^{-\lambda h_1} & (1 - \kappa - 2\lambda h_1)e^{-\lambda h_1} \\ -2i\lambda(\kappa - 1) & i(\kappa^2 - 1) & -2i\lambda(\kappa - 1) & i(1 - \kappa^2) \\ -2\lambda & \kappa - 1 & 2\lambda & \kappa - 1 \\ -1 & 0 & -1 & 0 \\ -i & i\kappa/\lambda & i & i\kappa/\lambda \end{bmatrix},$$

$$D'' = \begin{bmatrix} \Delta_1 & \Delta_2 & \Delta_3 & \Delta_4 \\ \Lambda_1 & \Lambda_2 & \Lambda_3 & \Lambda_4 \\ 1 & 1 & 1 & 1 \\ s_1 & s_2 & s_3 & s_4 \\ \Delta_1 e^{-m_1 h_2} & \Delta_2 e^{-m_2 h_2} & \Delta_3 e^{-m_3 h_2} & \Delta_4 e^{-m_4 h_2} \\ \Lambda_1 e^{-m_1 h_2} & \Lambda_2 e^{-m_2 h_2} & \Lambda_3 e^{-m_3 h_2} & \Lambda_4 e^{-m_4 h_2} \end{bmatrix},$$

with

$$\Delta_k = -i\lambda(3 - \kappa) + (1 + \kappa)m_k s_k, \quad \Lambda_k = m_k - i\lambda s_k, \quad k = 1, 2, 3, 4.$$

References

1. F. ERDOGAN, *Fracture mechanics of functionally graded materials*, Compos. Eng., **5** (7), 753–770, 1995.
2. S. SURESH, A.E. GIANNAKOPOULOS, J. ALCALÁ, *Spherical indentation of compositionally graded materials: Theory and experiments*, Acta Mater., **45** (4), 1307–1321, 1997.

3. S. SURESH, *Graded materials for resistance to contact deformation and damage*, Science, **292**, 2447–2451, 2001.
4. M.A. GULER, F. ERDOGAN, *Contact mechanics of two deformable elastic solids with graded coatings*, Mech. Mater., **38** (7), 633–647, 2006.
5. M.A. GULER, F. ERDOGAN, *The frictional sliding contact problems of rigid parabolic and cylindrical stamps on graded coatings*, Int. J. Mech. Sci., **49** (2), 161–182, 2007.
6. R. ELLOUMI, I. KALLEL-KAMOUN, S. EL-BORGI, *A fully coupled partial slip contact problem in a graded half-plane*, Mech. Mater., **42** (4), 417–428, 2010.
7. M.A. GULER, M. OZTURK, A. KUCUKSUCU, *The frictional contact problem of a rigid stamp sliding over a graded medium*, Key Eng. Mat., **681** (4), 155–174, 2016.
8. A.E. GIANNAKOPOULOS, P. PALLOT, *Two-dimensional contact analysis of elastic graded materials*, J. Mech. Phys. Solids, **48** (8), 1597–1631, 2000.
9. S. CHEN, C. YAN, P. ZHANG, H. GAO, *Mechanics of adhesive contact on a power-law graded elastic half-space*, J. Mech. Phys. Solids, **57** (9), 1437–1448, 2009.
10. Y.S. WANG, D. GROSS, *Analysis of a crack in a functionally gradient interface layer under static and dynamic loading*, Key Eng. Mat., **183–187**, 331–336, 2000.
11. L.L. KE, Y.S. WANG, *Two-dimensional contact mechanics of functionally graded materials with arbitrary spatial variations of material properties*, Int. J. Solids Struct., **43** (18), 5779–5798, 2006.
12. T.-L. LIU, Y.S. WANG, C. ZHANG, *Axisymmetric frictionless contact of functionally graded materials*, Arch. Appl. Mech., **78** (4), 267–282, 2008.
13. K.L. JOHNSON, *Contact Mechanics*, Cambridge Univ. Press, London, 1985.
14. S. EL-BORGI, R. ABDELMOULA, L. KEER, *A receding contact plane problem between a functionally graded layer and a homogeneous substrate*, Int. J. Solids Struct., **43**, 658–674, 2006.
15. S. EL-BORGI, S. USMAN, M.A. GÜLER, *A frictional receding contact plane problem between a functionally graded layer and a homogeneous substrate*, Int. J. Solids Struct., **51** (25–26), 4462–4476, 2014.
16. M. RHIMI, S. EL-BORGI, S.W. BEN, F.B. JEMAA, *A receding contact axisymmetric problem between a functionally graded layer and a homogeneous substrate*, Int. J. Solids Struct., **46**, 3633–3642, 2009.
17. G. ADIYAMAN, A. BIRINCI, E. ÖNER, M. YAYLACI, *A receding contact problem between a functionally graded layer and two homogeneous quarter planes*, Acta Mechanica, **227** (6), 1753–1766, 2016.
18. M. RHIMI, S. EL-BORGI, N. LAJNEF, *A double receding contact axisymmetric problem between a functionally graded layer and a homogeneous substrate*, Mech. Mater., **43** (12), 787–798, 2011.
19. J. YAN, X. LI, *Double receding contact plane problem between a functionally graded layer and an elastic layer*, Eur. J. Mech. A-Solid., **53**, 143–150, 2015.
20. T.-J. LIU, C. ZHANG, Y.-S. WANG, Y.-M. XING, *The axisymmetric stress analysis of double contact problem for functionally graded materials layer with arbitrary graded materials properties*, Int. J. Solids Struct., **96**, 229–239, 2016.

21. H. ADIBELLI, İ ÇÖMEZ, R. ERDÖL, *Receding contact problem for a coated layer and a half-plane loaded by a rigid cylindrical stamp*, Arch. Mech., **65** (3), 219–236, 2013.
22. M. YAYLACI, E. ÖNER, A. BIRINCI, *Comparison between analytical and ANSYS calculations for a receding contact problem*, J. Eng. Mech.–ASCE, **140** (9), 04014070, 2014.
23. H.J. CHOI, G.H. PAULINO, *Thermoelastic contact mechanics for a flat punch sliding over a graded coating/substrate system with frictional heat generation*, J. Mech. Phys. Solids, **56** (4), 1673–1692, 2008.
24. T.-J. LIU, Y.-M. XING, Y.-S. WANG, *The axisymmetric contact problem of a coating/substrate system with a graded interfacial layer under a rigid spherical punch*, Math. Mech. Solids, **21** (3), 383–399, 2016.
25. R. WHITE, *Asymptotic Analysis of Differential Equations*, Imperial College Press, Singapore, 2010.
26. F. ERDOGAN, G.D. GUPTA, *On the numerical solution of singular integral equations*, Q. Appl. Math., **29**, 525–534, 1972.
27. X. LI, *Boundary Value Problems and Related Problems*, World Scientific Publishing, Singapore, 2013.
28. J.M. ORTEGA, W.C. RHEINBOLDT, *Iterative Solution of Nonlinear Equations in Several Variables*, Society for Industrial and Applied Mathematics, Philadelphia, 1987.
29. V. VOLKAN, T.S. OZSAHIN, A. BIRINCI, R. ERDÖL, *A receding contact problem for an anisotropic elastic medium consisting of a layer and a half plane*, Int. J. Solids Struct., **44** (17), 5695–5710, 2007.

Received November 25, 2016; revised version February 23, 2017.
